

Article

Highly Water-Stable Zinc Based Metal–Organic Framework: Antibacterial, Photocatalytic Degradation and Photoelectric Responses

Congying Yuan ¹, Yadi Miao ¹, Yinhang Chai ^{2,3}, Xiaojun Zhang ¹, Xiaojing Dong ¹ and Ying Zhao ^{2,*}

¹ College of Life Science, Luoyang Normal University, Luoyang 471934, China; pingboyicy@163.com (C.Y.); myd17838906156@163.com (Y.M.); z2015797093@163.com (X.Z.); 13383799287@163.com (X.D.)

² Henan Province Function-Oriented Porous Materials Key Laboratory, College of Chemistry and Chemical Engineering, Luoyang Normal University, Luoyang 471934, China; chaiyinhangyh@163.com

³ College of Chemistry, Zhengzhou University, Zhengzhou 450001, China

* Correspondence: zhaoying_909@sina.com

Abstract: A reported water-stable Zn-MOF ($[\text{Zn}(\text{L})_2(\text{bpa})(\text{H}_2\text{O})_2] \cdot 2\text{H}_2\text{O}$, $\text{H}_2\text{L} = 5$ - $(2$ -cyanophenoxy) isophthalic acid has been prepared via a low-cost, general and efficient hydrothermal method. It is worth noting the structural features of Zn-MOF which exhibit the unsaturated metal site and the main non-covalent interactions including $\text{O} \cdots \text{H}$, $\text{N} \cdots \text{H}$ and π - π stacking interactions, which lead to strong antibacterial and good tetracycline degradation ability. The average diameter of the Zn-MOF inhibition zone against *Escherichia coli* and *Staphylococcus aureus* was 12.22 mm and 10.10 mm, respectively. Further, the water-stable Zn-MOF can be employed as the effective photocatalyst for the photodegradation of tetracycline, achieving results of 67% within 50 min, and it has good cyclic stability. In addition, the photodegradation mechanism was studied using UV-vis diffuse reflection spectroscopy (UV-VIS DRS) and valence-band X-ray photoelectron spectroscopy (VB-XPS) combined with the ESR profile of Zn-MOF, which suggest that $\cdot\text{O}_2^-$ is the main active species responsible for tetracycline photodegradation. Also, the photoelectric measurement results show that Zn-MOF has a good photocurrent generation performance under light. This provides us with a new perspective to investigate Zn-MOF materials as a suitable multifunctional platform for future environmental improvement applications.

Keywords: metal–organic framework; antibacterial ability; tetracycline degradation; photocurrent generation performance



Citation: Yuan, C.; Miao, Y.; Chai, Y.; Zhang, X.; Dong, X.; Zhao, Y. Highly Water-Stable Zinc Based Metal–Organic Framework: Antibacterial, Photocatalytic Degradation and Photoelectric Responses. *Molecules* **2023**, *28*, 6662. <https://doi.org/10.3390/molecules28186662>

Academic Editor: Liming Fan

Received: 5 August 2023

Revised: 1 September 2023

Accepted: 3 September 2023

Published: 16 September 2023



Copyright: © 2023 by the authors. Licensee MDPI, Basel, Switzerland. This article is an open access article distributed under the terms and conditions of the Creative Commons Attribution (CC BY) license (<https://creativecommons.org/licenses/by/4.0/>).

1. Introduction

Pathogens have a high incidence rate and mortality, which directly threaten human health and the development of the ecological environment [1–3]. For various infections caused by bacteria, antibiotic therapy seems to be a long-term effective strategy. However, the widespread use of antibiotics has led to severe bacterial resistance and even the emergence of superbugs. Based on this current situation, the development of new antibacterial materials has become an urgent focus in the fields of materials science and biochemistry [4–8]. Among the previously reported antibiotics, tetracycline was widely used for the treatment of infectious diseases in humans and animals [9,10]. Non-biodegradability can easily result in health problems for aquatic organisms and increase the risk of antibiotic-resistant pathogens. Therefore, it is of great significance to develop stable antibacterial and antibiotic-degrading materials for the sustainable development of biology [11–13].

Metal–organic frameworks (MOFs) are an important class of compounds in which organic bridging ligands connect metal ions or metal-containing nodes to form a three-dimensional coordination network with potential voids [14,15]. The key advantage of MOFs over other microporous species is their highly adjustable composition [16], which

can be achieved by using different metal ions or modifying organic linkers [17,18]. Due to their high surface area and open space, host–guest chemistry related to MOFs, such as energy-related technologies [19], heterogeneous catalysis [20], gas purification [21] and sensing [22], has been systemically studied. Because of the increasing number of multidrug-resistant bacteria in recent years and the residues of antibiotic drugs in the environment, there is increasing interest in developing new environmental applications of MOFs. In this regard, some transition metals [23–25] and metal nanoparticles (NPs) [26–28] have been extensively studied as antimicrobial agents and photocatalytic degraders. We also know that the degradable metal zinc has attracted the attention of researchers because it has a better degradation rate than magnesium and iron. Studies have shown that zinc has good biocompatibility in vivo, Zn^{2+} can promote cell growth and differentiation, and a high concentration of Zn^{2+} has certain antibacterial abilities. However, pure zinc does not display activity in vitro, and Zn^{2+} released by pure zinc is not enough to provide sufficient antibacterial activity [29]. Therefore, it has become an urgent problem to improve the surface bioactivity and cytocompatibility of zinc metal through the self-assembly of ligands and metals and to engender antibacterial properties and photocatalytic degradation properties.

Based on these questions, we used a case of water-stable Zn-MOF as previously reported by our research group [30] to study its antibacterial and photodegradation catalytic ability. Generally, molecular interactions and dynamics in the photocatalyst influence the activity, which in turn will be influenced by linker substitution. The aromatic carboxylic acid ligands can generate suitable electronic transitions, while self-assembly with zinc ions to form MOF can further improve stability and surface activity. Upon investigation, Zn-MOF has antibacterial properties and good photocatalytic degradation performance for tetracycline. The active substances easily produced by the catalyst were characterized by ESR and the mechanism of photocatalytic degradation was revealed. Finally, we also studied the photoelectric response performance.

2. Results

2.1. Antibacterial Properties of Zn-MOF

The results showed that Zn-MOF had inhibitory effects on both *Escherichia coli* and *Staphylococcus aureus*. The average diameter of the inhibitory zone of *Escherichia coli* was 12.22 mm, and that of *Staphylococcus aureus* was 10.10 mm, as shown in Figures 1 and 2. The different antibacterial effects of the materials on *Escherichia coli* and *Staphylococcus aureus* may be due to the fact that the cell wall of *Staphylococcus aureus* (Gram-positive bacteria) is thicker than that of *Escherichia coli* (Gram-negative bacteria). This makes it more difficult for Zn-MOF to enter the cells of *Staphylococcus aureus*, thus preventing the bacterial structure from being destroyed.

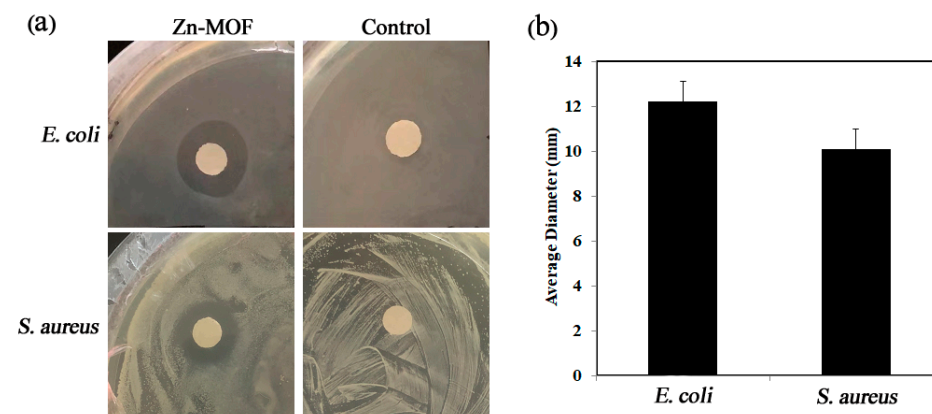


Figure 1. (a) Effect of Zn-MOF on bacteriostasis of *Escherichia coli* and *Staphylococcus aureus*. (b) Average diameter of Zn-MOF inhibition zone for two kinds of bacteria (mm).

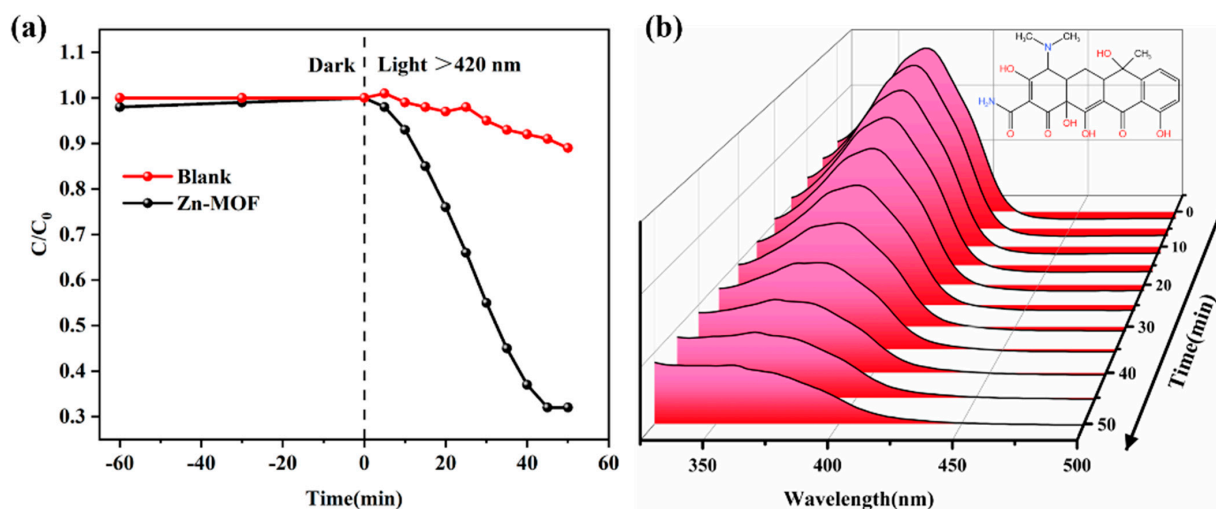


Figure 2. (a) Photodegradation of tetracycline with Zn-MOF under visible light. (b) UV absorption monitoring of tetracycline concentration with light time degradation process.

2.2. Photocatalytic Properties of Zn-MOF

Tetracycline, an antibiotic widely found in the environment, was used to evaluate the photocatalytic activity of Zn-MOF in this work. First, the photocatalytic performance of Zn-MOF was tested, and the photolysis efficiency reached about 67% within 50 min (Figure 2a). Meanwhile, the change in the ultraviolet absorption spectrum of tetracycline during the photodegradation process is shown in Figure 2b. With the increase in irradiation time, the characteristic absorption peak of tetracycline gradually decreases, and the decrease in the absorption peak intensity indicates that most tetracycline molecules can be degraded and no other substances are formed.

However, in a blank control test, only negligible tetracycline degradation was observed in the absence of a photocatalyst (Figure 2a). In addition, kinetic characterization was performed, and the results showed that the photodegradation data fit the pseudo-first-order kinetic model. Figure 3 shows the dynamic curve, and the calculation formula $-\ln(C_0/C_t) = kt$, where k , C_t and C_0 , respectively, represent the apparent rate constant of the reaction, the instantaneous concentration at time t and the initial concentration of tetracycline [31]. It is found that the degradation rate constant of Zn-MOF can be as high as 0.02627 min^{-1} , while that of the control group is 0.0024 min^{-1} , which represents a ten-fold increase. The results indicate that Zn-MOF has potential application value in removing tetracycline from an aqueous solution.

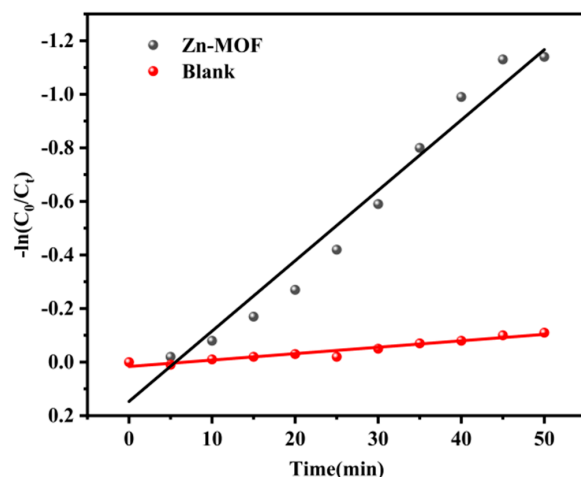


Figure 3. Kinetic rate constants of tetracycline degradation in the presence of Zn-MOF.

2.3. Cyclic Stability of Zn-MOF Photocatalysis

Cyclic stability is an important factor in evaluating the application of photocatalysts. Therefore, the stability performance of the photocatalyst was evaluated by comparing the degradation efficiency and the consistency of PXRD patterns before and after cyclic tests. After each cycle, the sample was cleaned with deionized water and dried. As shown in Figure 4a, the structure of the complex remained good after three cycles, and no obvious deactivation occurred. Meanwhile, in the third run, the degradation efficiency of tetracycline under visible light irradiation remained at 51.6% (Figure 4b), which indicated that Zn-MOF has good stability. At the same time, as shown in prior research [11,32], the phenomenon is basically consistent with that of relevant previous studies.

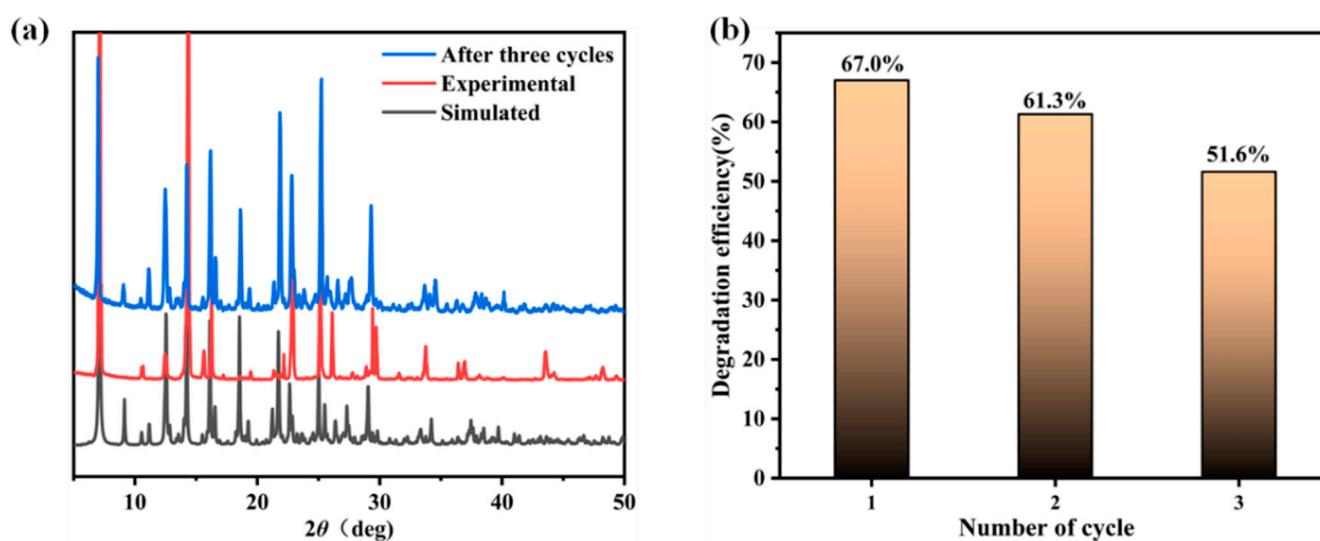


Figure 4. (a) PXRD pattern. (b) Recycling performance of Zn-MOF-degraded tetracycline.

2.4. Analysis of Active Components in Photodegradation of Zn-MOF

In order to study the active substances produced in photodegradation, we characterized the materials via electron spin resonance (ESR) spectroscopy with the trapping agent 5,5-dimethyl-1-pyrroline N-oxide (DMPO) and further investigated their photocatalytic properties, which provided support for the catalytic mechanism. As shown in Figure 5, under dark conditions, it can be clearly observed that Zn-MOF does not have DMPO·OH and DMPO·O₂[−] signals. However, the typical DMPO·OH (Figure 5a) and DMPO·O₂[−] (Figure 5b) adducts were detected under visible light compared to the signals under dark conditions, indicating the successful formation of the two active substances. In addition, the signal strength of DMPO·O₂[−] was significantly higher than that of DMPO·OH when comparing the signal strength of the two active substances produced. These results indicate that ·O₂[−] plays a key role in the photodegradation of tetracycline, while ·OH plays a secondary role.

2.5. Morphology Measurement and BET Surface Area Analysis

In order to clearly show the morphological characteristics of Zn-MOF, Figure 6a displays its SEM image. The particles are relatively regular with a cubic structure, and the crystal has a uniform size on the micrometer scale. Furthermore, the pore structure, pore characteristics and specific surface area of the Zn-MOF sample were studied using adsorption and desorption techniques under 77 K nitrogen atmosphere. As shown in Figure 6b, the isotherm of Zn-MOF showed type IV, and hysteresis curves of the complex appeared under high pressure (P/P_0), which proved that the pores in the structure were relatively concentrated [33]. Using the Barrett–Joyner–Halenda method, we found that the surface area and pore volume of Zn-MOF were 11.4087 m²/g and 44.64 × 10^{−3} cm³/g, respectively. The photocatalytic degradation can be related to different pathways. Although the small

specific surface area and pore size do not provide positive factors for the photocatalytic process, the performance of Zn-MOF could be interpreted based on its textural properties. In addition to the direct photocatalytic degradation of tetracycline molecules absorbed by Zn-MOF, photogenerated electron–hole pairs can generate highly oxidative species such as superoxide anions and hydroxyl radicals. These mobile radicals will indirectly degrade the tetracycline in the surrounding solution. Furthermore, it is speculated that the main non-covalent interactions exhibited by Zn-MOF are O...H and N...H interactions, suggesting that tetracycline molecules can interact with materials through these interactions, which play a key role in the degradation of tetracycline molecules.

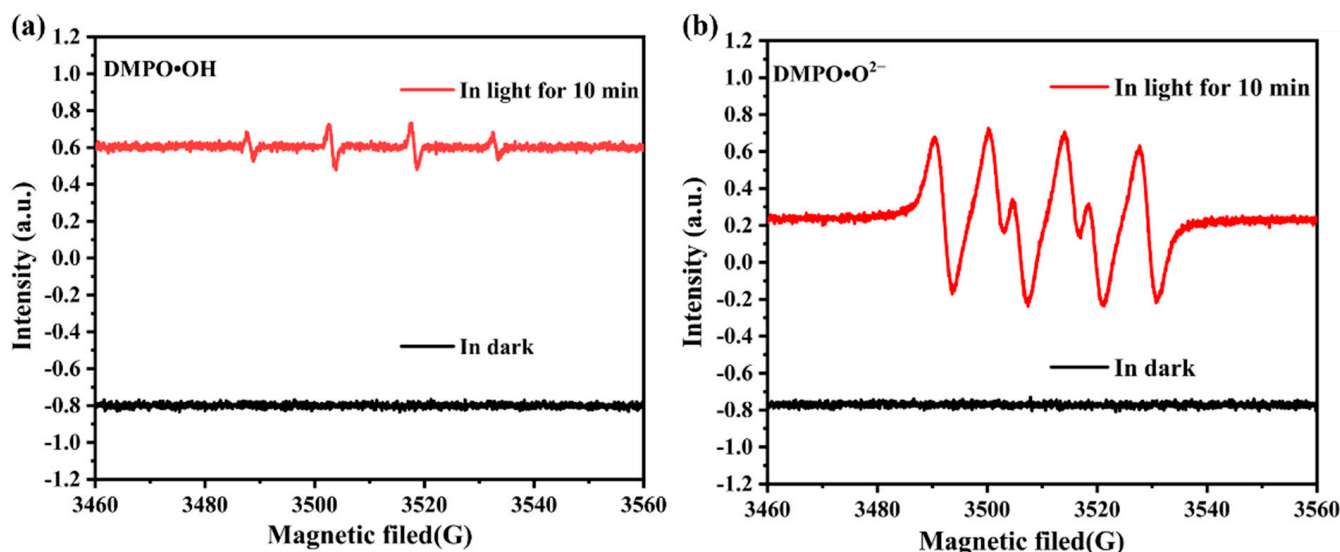


Figure 5. ESR spectra of (a) DMPO·OH, (b) DMPO·O₂[−].

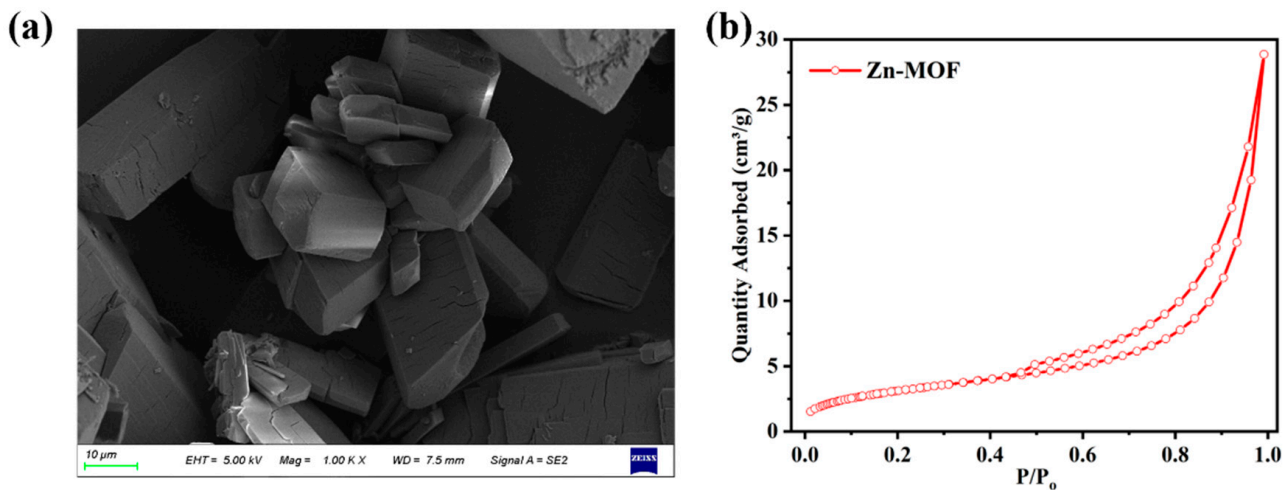


Figure 6. (a) SEM image of Zn-MOF. (b) Adsorption/desorption isotherm of Zn-MOF.

2.6. Possible Mechanism of Tetracycline Degradation

In order to more clearly analyze the production and action processes of hydroxyl radicals and superoxide radicals, we proposed a potential photodegradation mechanism based on the association between VB-XPS and UV-vis DRS analysis and ESR profiles. When illuminated by a photon with energy close to or higher than E_g (Zn-MOF), electrons (e^-) in the valence band (VB) will be excited and transferred to the conduction band (CB), ultimately causing the vacancy (h^+) to remain in the valence band. As shown in Figure 7, the VB (2.76 eV) potential of Zn-MOF is more favorable than the VB potential of water

molecules converting to hydroxyl radicals (2.38 eV vs. NHE) [34], resulting in visible light-generated holes (h^+) reacting with water molecules to form hydroxyl radicals ($\cdot\text{OH}$). At the same time, the CB potential of **Zn-MOF** (-1.15 eV) is more negative than the potential of oxygen conversion to superoxide free radicals (-0.33 eV vs. NHE) [35], which encourages the photoinduced electrons (e^-) to react with oxygen to form superoxide free radicals ($\cdot\text{O}_2^-$). However, from the mechanism diagram, we can also observe that the superoxide radical has a stronger production effect than the hydroxyl radical, which is consistent with the ESR spectrum.

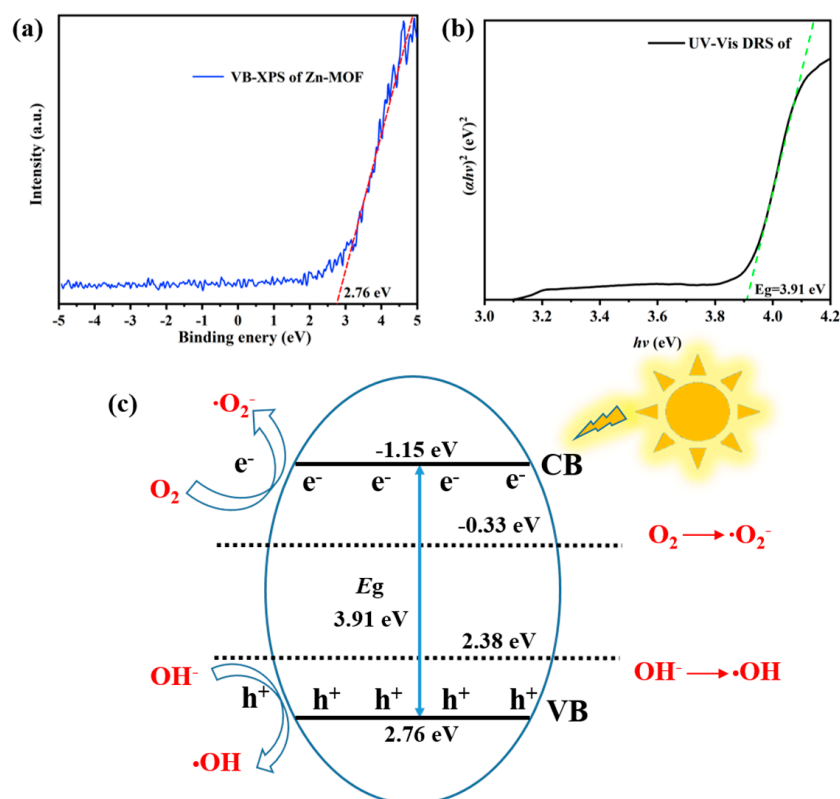


Figure 7. (a) VB-XPS spectra. (b) UV-vis DRS diagram. (c) Possible mechanism of tetracycline degradation.

2.7. Analysis of Photoelectric Response

The electrochemical workstation and the three-electrode system were jointly used to evaluate the photoelectric performance of **Zn-MOF**. According to the cyclic voltammetry curve (Figure 8a), it can be found that the working electrode has a strong photoelectric response to negative voltage, and its current density exceeds $20 \mu\text{A cm}^{-2}$ at a voltage of -0.6 V. In addition, under switching illumination (10 s) and a bias potential of 0.5 V, the working electrode exhibited a significant photoelectric response behavior (Figure 8c). Notably, periodic and persistent photocurrent signals are displayed in multiple on/off cycles. In order to further confirm the photoelectric response of the material, we also measured the photoelectric response at the opposite voltage -0.5 V bias voltage. Consistent with the cyclic voltammetry curve, the response is better at -0.5 V, which is about three times that under positive pressure (Figure 8d). In order to clarify the effect of additional light on the current of the working electrode, an electrochemical impedance spectroscopy (EIS) experiment was performed at a potential of -0.5 V (Figure 8b). Obviously, the addition of light can effectively reduce the charge transfer resistance.

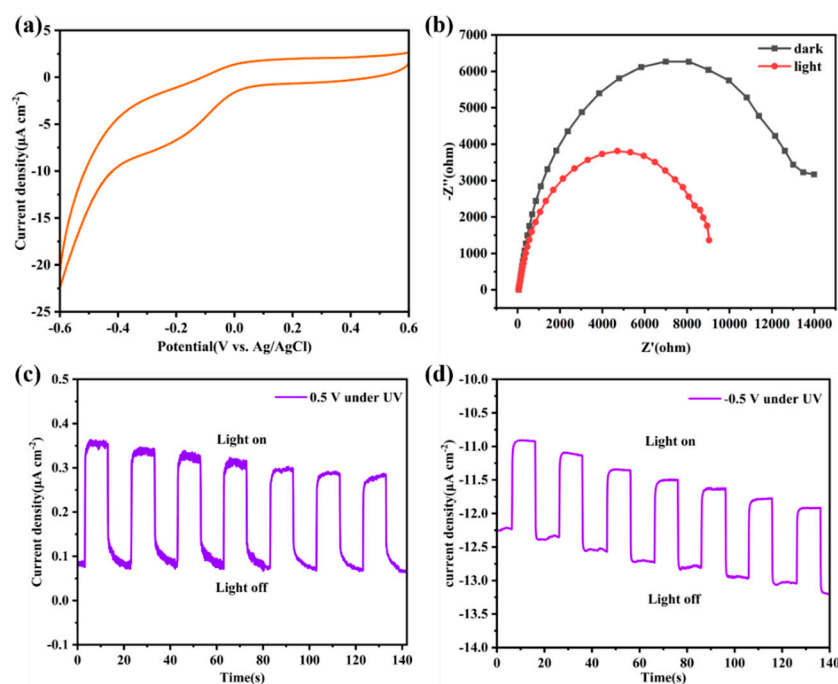


Figure 8. (a) Cyclic voltammetry of Zn-MOF. (b) Electrochemical impedance spectra (EIS) of Zn-MOF under dark irradiation. (c,d) Transient current density time curves of Zn-MOF under different bias potentials.

3. Experiment

3.1. Synthesis of $[Zn(L)_2(bpa)(H_2O)_2] \cdot 2H_2O$

A mixture of $Zn(OAc)_2 \cdot 2H_2O$ (0.1 mmol, 20 mg), 5-(2-cyanophenoxy) isophthalic acid (H_2L 0.1 mmol, 28 mg), 1,2-bis (4-pyridine)-ethane (bpa, 0.1 mmol, 16.8 mg) and H_2O (8 mL) was sealed in a 25 mL Teflon-lined reactor at 120 °C for 3 days. When cooled to room temperature, regular crystals of Zn-MOF were obtained [30].

3.2. Materials and Equipment

The raw materials are all commercially purchased and do not require further purification. The solvents used are all analytical-grade solvents. Subsequently, the ESR was collected with Bruker A300 (Billerica, MA, USA), and the UV-vis diffuse reflectance spectrum was recorded with Shimadzu UV-2600 UV-vis spectrophotometer (Kyoto, Japan). Powder X-ray diffraction (PXRD) patterns were obtained using a Bruker D8 Advance powder diffractometer using $Cu-K\alpha$ radiation ($\lambda = 1.5418 \text{ \AA}$) at a scanning rate of 0.2 s/step and a step size of 0.02 (2θ) at 40 kV and 40 mA.

3.3. Antibacterial Performance Test

This work evaluates the antibacterial effect of Zn-MOF via the bacteriostatic zone method. Gram-negative bacteria (*Escherichia coli*) and Gram-positive bacteria (*Staphylococcus aureus*) were selected as research objects to measure Zn-MOF antibacterial performance. The diffusion of the sample in the solid culture substrate was used to inhibit the growth of bacteria and form a transparent circular bacteriostatic zone centered around it.

Firstly, the prepared Zn-MOF sample was ground and dispersed in dimethyl sulfoxide (DMSO), and 6 mm circular filter paper with a diameter of pre-sterilized bacteria was placed in the prepared Zn-MOF solution. Then, under aseptic conditions, the prepared LB (Luria-Bertani) solid medium plate was placed on the ultra-clean worktable next to the flame of the alcohol lamp. A total of 50 μL bacteria solution was absorbed and added to the LB solid medium. The bacteria solution was evenly coated with the sterilized coating stick, the filter paper soaked in LB liquid medium, and the filter paper soaked in Zn-MOF solution was removed with tweezers. Finally, the sealed medium plate was placed in a constant

temperature incubator at 37 °C. After about 18 h of culture, it was taken out. A Vernier caliper was used to measure the diameter (in three directions) of the bacterial-inhibition zone centered on the sample, and its average value was taken as the experimental result.

3.4. Determination of Photocatalytic Activity

The photocatalytic performance of **Zn-MOF** on tetracycline was evaluated by using a 300 W xenon lamp equipped with a 420 nm filter to simulate the degradation of tetracycline. Firstly, the catalyst reached absorption–desorption equilibrium under dark conditions. The experimental method involved dispersing the ground photocatalyst (50 mg) in a tetracycline aqueous solution (20 ppm L⁻¹) and stirring continuously for 60 min under dark conditions. Then, the reaction solution was exposed to visible light, and the reaction solution (3 mL) was removed every 5 min and filtered through the filter head of a disposable PES filter with a diameter of 0.45 µm. The supernatant was then collected for UV analysis. The tetracycline concentration was monitored by measuring the absorption intensity of the maximum absorption wavelength ($\lambda = 357$ nm) with a Hitachi UV-visible spectrophotometer (UH-5300, Tokyo, Japan). Pollutant decomposition efficiency (η) [30] is calculated as follows:

$$\eta = \left(1 - \frac{C}{C_0}\right) \times 100\%$$

The concentration of pollutants after adsorption equilibrium is represented by C_0 , where C is the concentration of pollutants during irradiation. In order to evaluate the stability and reusability of **Zn-MOF**, cyclic photodegradation experiments were performed, and followed the same process as above. At the end of each cycle, the catalysts were collected via centrifugation, washed with deionized water and anhydrous ethanol, and dried under the same conditions for use in the next antibiotic degradation.

3.5. Photoelectric Response Measurement

In order to investigate the photoelectric ability of **Zn-MOF**, the photoelectric properties of the material were evaluated. The tests were performed on a CHI 660E electrochemical analyzer. In the standard three-electrode system, **Zn-MOF** powder-modified indium tin oxide (ITO) was used as the working electrode. The electrode coating area was 1.0 cm². A platinum wire electrode was used as the auxiliary electrode, Ag/AgCl was used as the reference electrode and 0.5 M Na₂SO₄ aqueous solution was used as the electrolyte. The system was carried out in a quartz glass reactor of about 50 cm³ and used a 300 W xenon lamp as a light source.

4. Conclusions

In summary, the multifunctional nature of **Zn-MOF** has been explored with regard to antibacterial properties, photocatalytic tetracycline degradation and photoelectric activity. **Zn-MOF** has an inhibitory effect on *Escherichia coli* and *Staphylococcus aureus*, the zinc ions in which can disturb the bacterial environmental metal balance and destroy the ion channels in the membrane. For tetracycline, **Zn-MOF** exhibits recyclable photocatalytic degradation. ESR testing demonstrates the importance of the production of active substances for photodegradation. At the same time, BET, SEM, UV-vis, VB-XPS and ESR spectra jointly explained the mechanism of photocatalytic degradation of tetracycline. Finally, the photoelectronic measurement results show that the **Zn-MOF**-modified electrode can produce higher photocurrent density under negative voltage response, and the photocurrent with adjustable frequency can be obtained by changing the lighting period of the switch and maintaining a certain intensity. This study provides a new perspective for exploring the development of MOF materials in antimicrobial, degradation and photoelectric directions.

Author Contributions: C.Y. and Y.M.: Synthesis of the title complex, antibacterial performance test; C.Y.: Writing—review and editing; Y.C.: Determination of photocatalytic activity; X.Z. and X.D.: completed photoelectric response measurement; Y.Z.: Supervision, writing—review and editing. All authors have read and agreed to the published version of the manuscript.

Funding: This work was supported by the National Natural Science Foundation of China (Grant No. 21801111): Natural Science Foundation of Henan Province (232300421232), Training Plan for Young Core Teachers in Higher Education of Henan Province (2021GGJS131) and the Key Scientific Research Projects of Higher Education of Henan Province for Grant 22A150049.

Institutional Review Board Statement: Not applicable.

Informed Consent Statement: Not applicable.

Data Availability Statement: Not applicable.

Conflicts of Interest: The authors declare no conflict of interest.

Sample Availability: Not applicable.

References

1. Li, X.; Zheng, H.; Chen, J.; Xu, M.; Bai, Y.; Liu, T. MIL-101 (Fe) @Ag Rapid Synergistic Antimicrobial and Biosafety Evaluation of Nanomaterials. *Molecules* **2022**, *27*, 3497. [[CrossRef](#)] [[PubMed](#)]
2. Lan, J.; Ge, J.; Yu, J.; Shan, S.; Zhou, H.; Fan, S.; Zhang, Q.; Shi, X.; Wang, Q.; Zhang, L.; et al. Structure of the SARS-CoV-2 spike receptor-binding domain bound to the ACE2 receptor. *Nature* **2020**, *581*, 215–220. [[CrossRef](#)] [[PubMed](#)]
3. Buder, S.; Schöfer, H.; Meyer, T.; Bremer, V.; Kohl, P.K.; Skaletz-Rorowski, A.; Brockmeyer, N. Bacterial sexually transmitted infections. *J. Dtsch. Dermatol. Ges.* **2019**, *17*, 287–315. [[CrossRef](#)] [[PubMed](#)]
4. Lázaro, I.; Forgan, R. Application of zirconium MOFs in drug delivery and biomedicine. *Coord. Chem. Rev.* **2019**, *380*, 230–259. [[CrossRef](#)]
5. Zhang, W.; Ye, G.; Liao, D.; Chen, X.; Lu, C.; Nezamzadeh-Ejhi, A.; Shahnawaz Khan, M.; Liu, J.; Pan, Y.; Dai, Z. Recent Advances of Silver-Based Coordination Polymers on Antibacterial Applications. *Molecules* **2022**, *27*, 7166. [[CrossRef](#)]
6. Taheri-Ledari, R.; Tarinsun, N.; Qazi, F.; Heidari, L.; Saeidirad, M.; Ganjali, F.; Ansari, F.; Hassanzadeh-Afruzi, F.; Maleki, A. Vancomycin-Loaded Fe₃O₄/MOF-199 Core/Shell Cargo Encapsulated by Guanidylated-β-Cyclodextrine: An Effective Antimicrobial Nanotherapeutic. *Inorg. Chem.* **2023**, *62*, 2530–2547. [[CrossRef](#)]
7. Zhou, Z.; Wang, T.; Hu, T.; Cheng, C.; Yu, S.; Li, H.; Liu, S.; Ma, L.; Zhao, M.; Liang, R.; et al. Facile Synthesis of 2D Al-TCPP MOF Nanosheets for Efficient Sonodynamic Cancer Therapy. *Mater. Chem. Front.* **2023**, *7*, 1684–1693. [[CrossRef](#)]
8. Xue, B.; Geng, X.; Cui, H.; Chen, H.; Kang, Z.; Chen, H.; Li, H.; Zhou, Z.; Zhao, M.; Tan, C.; et al. Size Engineering of 2D MOF Nanosheets for Enhanced Photodynamic Antimicrobial Therapy. *Chin. Chem. Lett.* **2023**, *34*, 108140. [[CrossRef](#)]
9. Maleki, A.; Shahbazi, M.; Alinezhad, V.; Santos, H. The Progress and prospect of zeolitic imidazolate frameworks in cancer therapy, antibacterial activity, and biomineralization. *Adv. Healthc. Mater.* **2020**, *9*, 2000248. [[CrossRef](#)]
10. Karimi, R.; Beheshti, S.; Akhbari, K.; Morsali, A. Investigation of reasons for metal–organic framework’s antibacterial activities. *Polyhedron* **2018**, *156*, 257–278. [[CrossRef](#)]
11. Tan, G.; Jia, R.; Zhao, X.; Guo, Y.; Zhang, L.; Wang, X.; Wang, J.; Feng, X.; Li, B.; Wang, L. Fabrication of Two Isomorphic and Hyperstable Rare Earth-Based Metal–Organic Frameworks with Efficient Ratiometric Probe and Photocatalytic Performances. *Inorg. Chem.* **2022**, *61*, 11866–11878. [[CrossRef](#)]
12. Zhang, Y.; Zhou, J.; Chen, X.; Wang, L.; Cai, W. Coupling of heterogeneous advanced oxidation processes and photocatalysis in efficient degradation of tetracycline hydrochloride by Fe-based MOFs: Synergistic effect and degradation pathway. *Chem. Eng. J.* **2019**, *369*, 745–757. [[CrossRef](#)]
13. Liu, Y.; Kong, J.; Yuan, J.; Zhao, W.; Zhu, X.; Sun, C.; Xie, J. Enhanced photocatalytic activity over flower-like sphere Ag/Ag₂CO₃/BiVO₄ plasmonic heterojunction photocatalyst for tetracycline degradation. *Chem. Eng. J.* **2018**, *331*, 242–254. [[CrossRef](#)]
14. Umemura, A.; Diring, S.; Furukawa, S.; Uehara, H.; Tsuruoka, T.; Kitagawa, S. Morphology design of porous coordination polymer crystals by coordination modulation. *J. Am. Chem. Soc.* **2011**, *133*, 15506–15513. [[CrossRef](#)] [[PubMed](#)]
15. Batten, S.; Champness, N.; Chen, X.; Garcia-Martinez, J.; Kitagawa, S.; Öhrström, L.; O’Keeffe, M.; Suh, M.; Reedijk, J. Coordination polymers, metal-organic frameworks and the need for terminology guidelines. *CrystEngComm* **2012**, *14*, 3001–3004. [[CrossRef](#)]
16. Deng, H.; Grunder, S.; Cordova, K.; Valente, C.; Furukawa, H.; Hmadeh, M.; Gándara, F.; Whalley, A.; Liu, Z.; Asahina, S.; et al. Large-Pore apertures in a series of metal-organic frameworks. *Science* **2012**, *336*, 1018–1024. [[CrossRef](#)]
17. Long, J.; Yaghi, O. The pervasive chemistry of metal-organic frameworks. *Chem. Soc. Rev.* **2009**, *38*, 1213–1214. [[CrossRef](#)] [[PubMed](#)]
18. Zhou, H.; Kitagawa, S. Metal-organic frameworks (MOFs). *Chem. Soc. Rev.* **2014**, *43*, 5415–5418. [[CrossRef](#)]
19. Choi, K.; Park, J.; Kang, J. Nanocrystalline MOFs embedded in the crystals of other MOFs and their multifunctional performance for molecular encapsulation and energy-carrier storage. *Chem. Mater.* **2015**, *27*, 5088–5093. [[CrossRef](#)]

20. Corma, A.; García, H.; Llabrés, F.; Xamena, I. Engineering metal organic frameworks for heterogeneous catalysis. *Chem. Rev.* **2010**, *110*, 4606–4655. [[CrossRef](#)]
21. Li, J.; Kuppler, R.; Zhou, H. Selective gas adsorption and separation in metal–organic frameworks. *Chem. Soc. Rev.* **2009**, *38*, 1477–1504. [[CrossRef](#)] [[PubMed](#)]
22. Kreno, L.; Leong, K.; Farha, O.; Allendorf, M.; Van Duyne, R.; Hupp, J. Metal–organic framework materials as chemical sensors. *Chem. Rev.* **2012**, *112*, 1105–1125. [[CrossRef](#)]
23. Santo, C.E.; Quaranta, D.; Grass, G. Antimicrobial metallic copper surfaces kill *Staphylococcus haemolyticus* via membrane damage. *Microbiologyopen* **2012**, *1*, 46–52. [[CrossRef](#)] [[PubMed](#)]
24. Casey, A.; Adams, D.; Karpanen, T.; Lambert, P.; Cookson, B.; Nightingale, P.; Miruszenko, L.; Shillam, R.; Christian, P.; Elliott, T. Role of copper in reducing hospital environment. *J. Hosp. Infect.* **2010**, *74*, 72–77. [[CrossRef](#)] [[PubMed](#)]
25. Jaros, S.W.; Król, J.; Bażanów, B.; Poradowski, D.; Chrószcz, A.; Nesterov, D.S.; Kirillov, A.M.; Smoleński, P. Antiviral, antibacterial, antifungal, and cytotoxic silver (I) BioMOF assembled from 1, 3, 5-triaza-7-phoshaadamantane and pyromellitic acid. *Molecules* **2020**, *25*, 2119. [[CrossRef](#)] [[PubMed](#)]
26. Chermousova, S.; Epple, M. Silver as antibacterial agent: Ion, nanoparticle, and metal. *Angew. Chem. Int. Ed.* **2013**, *52*, 1636–1653. [[CrossRef](#)]
27. Seyedpour, S.; Dadashi Firouzjaei, M.; Rahimpour, A.; Zolghadr, E.; Shamsabadi, A.; Das, P.; Afkhami, F.; Sadzadeh, M.; Tiraferri, A.; Elliott, M. Toward sustainable tackling of biofouling implications and improved performance of TFC FO membranes modified by Ag-MOF nanorods. *ACS Appl. Mater. Interfaces* **2020**, *12*, 38285–38298. [[CrossRef](#)]
28. Zhou, Y.; Yang, Q.; Zhang, D.; Gan, N.; Li, Q.; Cuan, J. Detection and removal of antibiotic tetracycline in water with a highly stable luminescent MOF. *Sens. Actuators B* **2018**, *262*, 137–143. [[CrossRef](#)]
29. Yang, H.; Wang, C.; Liu, C.; Chen, H.; Wu, Y.; Han, J.; Jia, Z.; Lin, W.; Zhang, D.; Li, W.; et al. Evolution of the degradation mechanism of pure zinc stent in the one-year study of rabbit abdominal aorta model. *Biomaterials* **2017**, *145*, 92–105. [[CrossRef](#)]
30. Chai, Y.; Liu, X.; Cui, Z.; Zhao, Y.; Ma, L.; Zhao, B. Design and syntheses of two luminescent metal-organic frameworks for detecting nitro-antibiotic, Fe^{3+} and $\text{Cr}_2\text{O}_7^{2-}$. *J. Solid State Chem.* **2022**, *312*, 123211. [[CrossRef](#)]
31. Ding, S.; Mao, D.; Yang, S.; Wang, F.; Meng, L.; Han, M.; He, H.; Sun, C.; Xu, B. Graphene-analogue h-BN coupled Bi-rich $\text{Bi}_4\text{O}_5\text{Br}_2$ layered microspheres for enhanced visible-light photo-catalytic activity and mechanism insight. *Appl. Catal. B* **2017**, *210*, 386–399. [[CrossRef](#)]
32. Wang, F.; Xue, R.; Ma, Y.; Ge, Y.; Wang, Z.; Qiao, X.; Zhou, P. Study on the performance of a MOF-808-based photocatalyst prepared by a microwave-assisted method for the degradation of antibiotics. *RSC Adv.* **2021**, *11*, 32955–32964. [[CrossRef](#)] [[PubMed](#)]
33. Shen, L.; Wu, W.; Liang, R.; Lin, R.; Wu, L. Highly Dispersed Palladium Nanoparticles Anchored on $\text{UiO-66}(\text{NH}_2)$ Metal-Organic Framework as a Reusable and Dual Functional Visible-Light-Driven Photocatalyst. *Nanoscale* **2013**, *5*, 9374. [[CrossRef](#)]
34. Zhou, E.; Li, B.; Chen, W.; Luo, Z.; Liu, J.; Singh, A.; Kumar, A.; Jin, J. Photocatalytic degradation of organic dyes by a stable and biocompatible Zn(II) MOF having ferulic acid: Experimental findings and theoretical correlation. *J. Mol. Struct.* **2017**, *1149*, 352–356. [[CrossRef](#)]
35. Zhang, X.; Wang, J.; Dong, X.; Lv, Y. Functionalized metal-organic frameworks for photocatalytic degradation of organic pollutants in environment. *Chemosphere* **2020**, *242*, 125144. [[CrossRef](#)] [[PubMed](#)]

Disclaimer/Publisher’s Note: The statements, opinions and data contained in all publications are solely those of the individual author(s) and contributor(s) and not of MDPI and/or the editor(s). MDPI and/or the editor(s) disclaim responsibility for any injury to people or property resulting from any ideas, methods, instructions or products referred to in the content.